Journal of GeoEngineering, Vol. 19, No. 1, pp. 047-058, March 2024
http://dx.doi.org/10.6310/jog.202403_19(1).4

NUMERICAL AND EXPERIMENTAL STUDY ON THE BEHAVIOR OF PILES SUBJECTED TO LIQUEFACTION-INDUCED LATERAL SPREADING

Yung-Yen Ko [1*] and Pei-Jou Chang [2]

ABSTRACT

Soil liquefaction is a destructive geotechnical hazard during earthquakes which causes not only ground settlement and foundation bearing capacity reduction but also lateral spreading of the ground. Lateral spreading can be harmful to embedded structures such as piles and hence may dominate the seismic design of piles. In this study, the behavior of piles subjected to liquefaction-induced lateral spreading was characterized by investigating a pile damage case during the 1964 Niigata, Japan earthquake. Firstly, both flow displacement and flow pressure approaches for modelling of lateral spreading and the beam on nonlinear Winkler foundation method for modeling of pile-soil interaction were adopted to numerically simulate the reality and an existing centrifuge test of the case. Then, a 1 g scaled physical model test was performed through compulsorily displacing a model ground which was liquefied by upward seepage to approximate the action of lateral spreading on the pile. The obtained results were compared with those from the field observations and existing study concerning the deformation, moment and soil reaction distribution, and damage mode of the pile. It was shown that the flow displacement approach better approximated the investigated case in which the pile penetration depth into the non-liquefied base layer was relatively small. The analyzed moment and soil reaction distribution along the pile were closer to those observed in the tests, leading to flexural damage of the pile near the interface of liquefied and non-liquefied layers just like the reality.

Key words: Soil liquefaction, lateral spreading, pile-soil interaction, beam on nonlinear Winkler foundation (BNWF), 1 g scaled physical model test.

1. INTRODUCTION

Soil liquefaction is a phenomenon that the strength and stiffness of a soil is degraded owing to the buildup of excess pore water pressure caused by dynamic actions such as earthquakes. It may reduce both vertical and lateral bearing capacity of pile foundations. Furthermore, as the ground is liquefied, lateral spreading of its near-surface part may occur, and consequently the embedded piles may be damaged due to ground displacement. For example, during the 1964 Niigata earthquake (M_w = 7.6), which is generally recognized to awake geotechnical engineers to the destructiveness of soil liquefaction as a geotechnical hazard during earthquakes, pile breakage was caused to the Niigata Family Court House and the NHK (Japan Broadcasting Corporation) building in the area suffering remarkable lateral spreading in Niigata City (Hamada 1992). The 1995 Kobe earthquake (M_w = 6.9) also caused severe lateral spreading in the Port of Kobe, leading to damage of precast concrete (PC) piles of a waterfront building and steel pipe piles of a pile-supported wharf in terms of flexural failure and local buckling, respectively (Tokimatsu and Asaka 1998; PIANC 2001). Consequently, lateral spreading can be critical to the seismic design of piles installed in liquefiable ground and hence becomes an issue necessary to be studied.

To this end, the present study aimed to numerically and experimentally investigate the mechanical behavior of piles under the influence of soil liquefaction-induced lateral spreading. A historical case of pile damage due to lateral spreading during the 1964 Niigata, Japan earthquake and an associated centrifuge physical model test were selected for demonstration. The Winkler foundation method (namely, a beam supported by soil springs), which is common in engineering practice, was utilized for pile-soil interaction analysis considering the nonlinearity of both soil and pile. Two loading modes that have been widely applied to simulate the action of lateral spreading, including the flow displacement and flow pressure approaches, were adopted. The analysis conditions were specified based on the reality and test configurations, respectively. To more realistically examine the pile response, a 1 g scaled physical model test was further performed. In this test, the action of lateral spreading on the pile was approximated by compulsorily displacing a model ground which was partially liquefied through controlled upward seepage. Based on the presented results, the behavior of piles subjected to lateral spreading can be better understood, and the practicability of the numerical modelling for assessing the performance of piles against lateral spreading can be evaluated, which are beneficial to the seismic design of pile foundations.

2. PILE DAMAGE CASE OF NIIGATA FAMILY COURT HOUSE DURING 1964 NIIGATA EARTHQUAKE

2.1 Field Observations

This study adopted the pile failure cases of the Niigata Family

Manuscript received November 11, 2023; revised January 23, 2024; accepted January 24, 2024.
[1*] Associate Professor (corresponding author), Department of Civil Engineering, National Cheng Kung University, Tainan, Taiwan (e-mail: yyko@ncku.edu.tw).
[2] Former Graduate Student, Department of Civil Engineering, National Cheng Kung University, Tainan, Taiwan.

Court House (abbreviated as NFCH hereafter) caused by the lateral spreading during the 1964 Niigata earthquake. This is because its two piles were excavated as the building was reconstructed 25 years after the quake and hence their failure modes were revealed (Hamada 1992), as depicted in Fig. 1, making in-depth investigation possible.

The two piles were both PC piles with an outer diameter of 35 cm, a thickness of 7.5 cm, and pile tip depths of 7 m and 9 m, respectively. The ground of this site has SPT-N values less than 10 down to a depth of nearly 8 m (Fig. 1) and was estimated liquefied from the groundwater table, which was at a depth of 1.7 m at boring (Hamada 1992) and somewhere between 2.5 and 3 m in 1964 (Dobry *et al.* 2003), to a depth of 8.5 m (Hamada 1992). Therefore, Pile #1 did not penetrate the non-liquefied firm base layer, whereas Pile #2 did.

The permanent displacement of the ground surface measured in the vicinity of NFCH was 1-2 m, leading to pile head displacements of Piles #1 and #2 of about 50 cm and 70 cm (Fig. 1(b)), respectively. Pile #1 suffered some flexural deformation and cracks near the groundwater table, *i.e.,* the interface of the non-liquefied crust and liquefied layers. On the other hand, Pile #2 was severely damaged at two locations. The upper one was also near the groundwater table, where the concrete was crushed, and the steel rebars were remarkably bent due to loss of confinement. The lower one was in an about 2-m range right above the interface of the liquefied and non-liquefied base layers, where many horizontal cracks and considerable rotation were induced by large bending moments. Moreover, a slight shear displacement was noticed at the upper damage of Pile #2, implying the different moving tendency of the crust and liquefied layers. In general, the piles in this case suffered more damage at the interfaces of non-liquefied and liquefied layers as subjected to lateral spreading, especially the crust layer-liquefied layer interface.

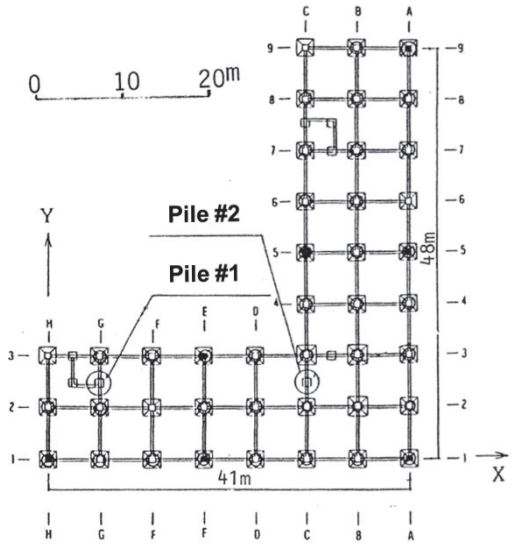

(a) Foundation layout

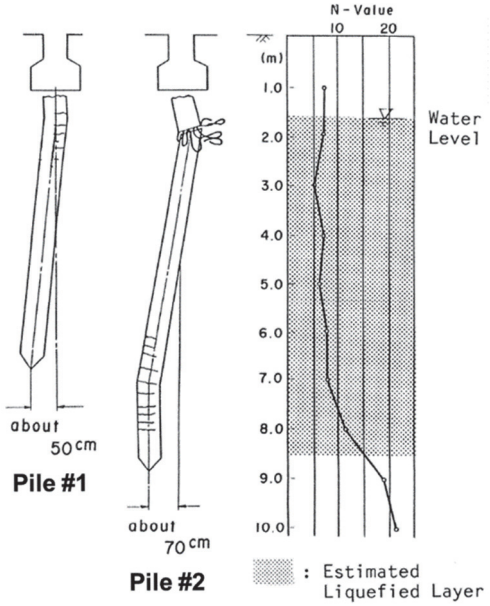

(b) Failure modes of piles and SPT-N values of the ground at the site

Fig. 1 NFCH pile damage case (after Hamada 1992)

2.2 Centrifuge Physical Model Test (Dobry *et al.* 1996)

Dobry *et al.* (1996) conducted a 50 g centrifuge shaking table test on Pile #2 of NFCH, as shown in Fig. 2. A three-layer (upper cemented sand, Nevada sand, and lower cemented sand layers to represent crust, liquefied, and firm base layers) sandy model ground was contained by a laminar box that was inclined 2° to the horizontal to cause lateral spreading during shaking. The model pile was made of a polyetherimide (PEI) rod with a diameter of 0.95 cm. It had an embedded length of 20 cm and was simplified to a free-head and end-fixed status. At a 50 g centrifugal acceleration, a pile with a diameter of 47.5 cm, a section rigidity (E_pI_p, where E_p and I_p denote Young's modulus and the cross-sectional moment of inertia of pile) of 8,000 kN-m^2, and an embedded length of 10 m (in prototype scale) was simulated. Notably, this E_pI_p value is between the initial E_pI_p (18,000 kN-m^2) and the secant E_pI_p after cracking (4,500 kN-m^2) of the real pile; hence, it can be regarded as an effective stiffness after slight damage. Moreover, this model pile remained elastic during the test owing to the high yield strain of PEI (~7%). The obtained pile and ground displacement as well as the moment distribution along the pile are given in Fig. 3. The model ground showed an 80 cm displacement of the crust layer and a linear displacement profile in the liquefied layer (Fig. 3(a)), making a pile head displacement of 95 cm. The moment distribution (Fig. 3(b)) exhibited a double-curvature feature of the pile due to the constraint of both crust and firm base layers as well as the end fixity.

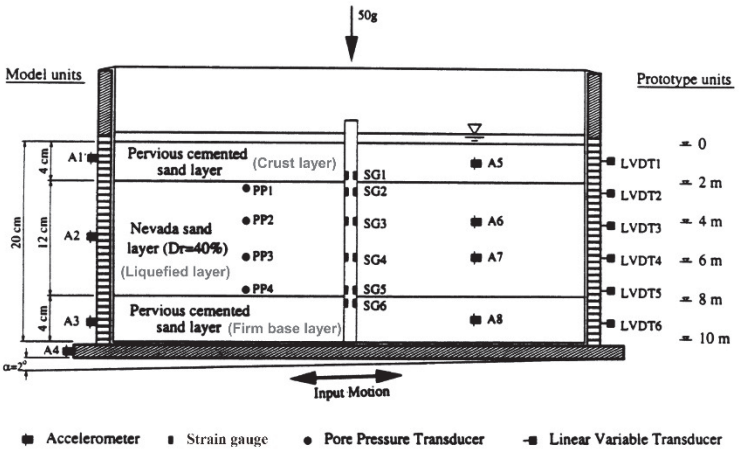

Fig. 2 Configurations of centrifuge modelling of lateral spreading on Pile #2 of NFCH (after Dobry *et al.* 1996)

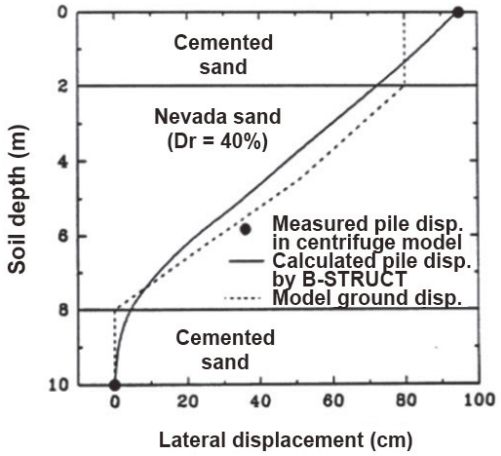

(a) Lateral displacement of the ground and pile

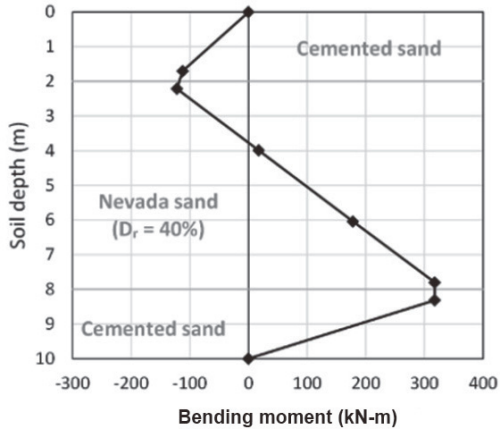

(b) Bending moment distribution along the pile

Fig. 3 Results of centrifuge modelling of Pile #2 of NFCH (in prototype scale) at the end of shaking (after Dobry *et al.* 1996)

3. METHODOLOGY

3.1 Numerical Pile-Soil Interaction Analysis

3.1.1 Beam on Nonlinear Winkler Foundation (BNWF) Method

The Winkler foundation model is widely used for the modelling of pile-soil system, in which the pile is simulated by beam elements, and the soil reaction is accounted for by spring elements spread along the pile (so-called soil springs), as shown in Fig. 4.

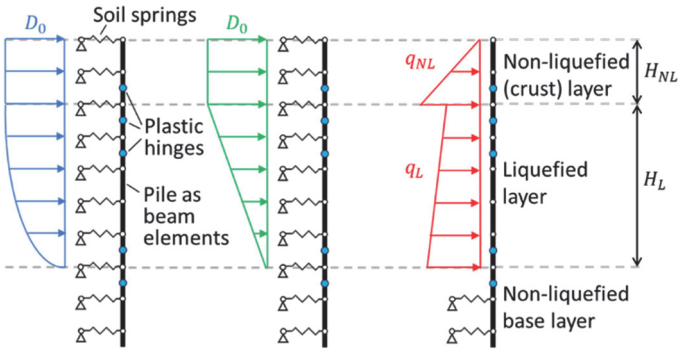

(a) Flow displacement – cosine profile (b) Flow displacement – linear profile (c) Flow pressure

Fig. 4 Modelling of pile-soil system and action of lateral spreading

For laterally loaded piles, the resistance is mainly attributed to the shallower soil layers for the larger pile displacement there. However, shallower soil layers are generally weaker and may show certain nonlinearity at a small deformation. Therefore, when Winkler foundation model is applied to a laterally loaded pile, the nonlinearity of soil is usually included. This is the so-called beam on nonlinear Winkler foundation (BNWF) method. The nonlinear soil spring is usually represented by the relationship of soil reaction (p) and the lateral displacement (y), namely, the p-y curve. In this study, the elastic-plastic p-y curves suggested in RTRI (2012) were adopted. Two parameters to define the p-y curve at a specific depth were determined according to the corresponding blow counts of the standard penetration test (SPT-N value) and the friction angle of soil (ϕ), including the subgrade reaction coefficient k_h as the slope of the linear part of p-y curves and the upper bound of soil reaction p_y, as depicted in Eq. (1).

$$k_h = 3.6 E_S D_p^{-\frac{3}{4}} \quad (\text{kN/m}^3) \tag{1a}$$

$$p_y = \alpha_h \sigma'_v \tan^2\left(45° + \frac{\phi}{2}\right) \quad (\text{kPa}) \tag{1b}$$

where E_S is the Young's modulus of soil, which can be approximated by E_S = 1540 (SPT-N) (in kPa), D_p is the pile diameter, α_h is the shape factor accounting for the effect of 3-D failure wedge of soil and can be assumed as 3.0, and σ'_v is the effective overburden pressure of soil (in kPa, with a lower bound of 50 kPa). The ϕ value can be determined also following RTRI (2012):

$$\phi = 1.85\left(\frac{\text{SPT-N}}{\sigma'_v/100 + 0.7}\right)^{0.6} + 26 \quad (\text{degree}) \tag{2}$$

Moreover, the reduction factor (D_E) corresponding to its liquefaction resistance (AIJ 2001) was used to account for the liquefaction-induced degradation of p-y curves. Then, the soil parameters for analysis were determined based on the SPT-N values of the NFCH site (Fig 1(b)) together with the assumptions that the groundwater table during the earthquake was at a depth of 2 m, liquefaction occurred in a depth range of 2-8.5 m, and the dry and saturated unit weights of soil are constantly 17.0 and 19.6 kN/m^3, as listed in Table 1.

A lateral loaded piles may suffer flexural failure because it may experience considerable moment. Hence, the distributed plastic hinge method (Chiou *et al.* 2009) is utilized to account for this possible flexural damage. This method is to insert multiple plastic hinges evenly distributed along the expected plastic zone of the pile (Fig. 4) with the plastic hinge length specified as the spacing between hinges. This is because the location of maximum moment may vary as the nonlinearity of supporting soil develops. The properties of plastic hinges on piles were defined by moment-curvature (M-ϕ) curves as shown in Fig. 5, where M_{cr}, M_y, and M_u denote cracking, yielding, and ultimate moments of the cross section of the pile, and ϕ_{cr}, ϕ_y, and ϕ_u are their corresponding curvature. Figure 5 can be regarded as the criteria of different levels of flexural failure of the pile. As the moment in the pile at a certain depth equals or exceeds the moment of a specific damage level, the pile damage there has reached this level.

Table 1 Parameters of soil for analysis

z (m)	SPT-N	k_h (kN/m^3)	ϕ (°)	p_y (kPa)	D_E
1.0	7	85199	31	159.3	1.0
2.0	7	85199	31	318.7	0.5
3.0	5	60857	30	394.3	0.1
4.0	7	85199	31	502.5	0.1
5.0	6	73028	30	594.5	0.1
6.0	8	97371	31	686.4	0.1
7.0	8	97371	31	778.4	0.1
8.0	11	133885	32	906.7	0.1
9.0	19	231255	34	1089.5	1.0
10.0	22	267769	34	1193.6	1.0

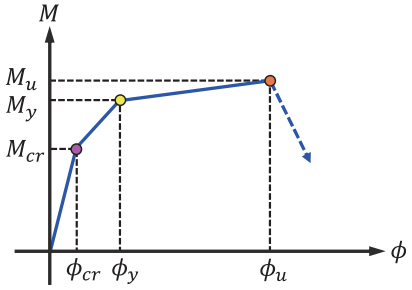

Fig. 5 Moment-curvature curve to define plastic hinges on piles

3.1.2 Modelling of Liquefaction-Induced Lateral Spreading in BNWF Method

The action of a laterally spreading ground during liquefaction on an embedded pile can be regarded as a moving soil body leaning against the pile and is more harmful if there is a non-liquefied crust layer due to its more significant interaction with the pile. In the analysis using the BNWF method for the pile response induced by this action, it can be modeled by the dynamic soil reaction calculated by free-filed ground acceleration and excess pore water pressure from effective-stress ground response analysis, such as Lin *et al.* (2006). Nevertheless, two quasi-static approaches are more commonly used in engineering practice for the modelling of laterally spreading and were both adopted in this study, as introduced below.

The first is the flow displacement approach. The predetermined free-field ground displacement profile due to lateral spreading is applied to the support ends of the soil springs (other than those attached to the pile), as depicted in Figs. 4(a) and 4(b). Notably, the *p-y* curves of liquefiable soil may need to be degraded to account for the difference in the actions of crust layer and liquefied layer. Then, a displacement-controlled analysis can be accordingly performed for the pile response. Brandenberg *et al.* (2007) used this approach to simulate a centrifuge physical model test on the pile-soil interaction in a laterally spreading ground (Brandenberg *et al.* 2005) and obtained the displacement and moment distribution of the pile as well as the soil reaction distribution that approximated the test results. Furthermore, Ashford *et al.* (2011) recommended this approach for the seismic design of piles subjected to liquefaction-induced lateral spreading.

Two different flow displacement profiles were used in this study. One is a cosine function with depth in the liquefied layer and constant in the crust layer proposed by Tokimatsu and Asaka (1998), as shown in Fig. 4(a), which was also observed in the 1 g full-scale shaking table test of Dobry *et al.* (2011). The displacement at a specific depth z, $D(z)$, can be expressed as:

$$D(z) = D_0 \quad \text{for } 0 \le z < H_{NL} \tag{3a}$$

$$D(z) = D_0 \cos\left[\frac{\pi(z - H_{NL})}{2H_L}\right] \quad \text{for } H_{NL} \le z < H_{NL} + H_L \tag{3b}$$

where D_0 is the ground surface displacement; H_{NL} and H_L are the thicknesses of the non-liquefied crust and liquefied layers, respectively.

The other displacement profile is linear in the liquefied layer and constant in the crust layer, as shown in Fig. 4(b), which was also observed in some physical model tests, such as Dobry *et al.* (1996) and Motamed *et al.* (2013). In this profile, $D(z)$ can be expressed as:

$$D(z) = D_0 \quad \text{for } 0 \le z < H_{NL} \tag{4a}$$

$$D(z) = D_0 \left(\frac{H_L + H_{NL} - z}{H_L}\right) \quad \text{for } z_w \le z < H_{NL} + H_L \tag{4b}$$

The second approach for modelling of lateral spreading is the flow pressure approach proposed by JRA (2012). The action of laterally spreading ground is represented by the passive pressure of the crust layer and the flow pressure of the liquefied layer directly imposed on the pile, as defined by Eq. (5):

$$q_{NL}(z) = c_s\, c_{NL}\, K_P\, \gamma_{NL}\, z \quad \text{for } 0 \le z < H_{NL} \tag{5a}$$

$$q_L(z) = c_s\, c_L[\gamma_{NL} H_{NL} + \gamma_L (z - H_{NL})] \quad \text{for } z_w \le z < H_{NL} + H_L \tag{5b}$$

where K_P is the passive earth pressure coefficient; γ_{NL} and γ_L are the unit weights of the non-liquefied crust and liquefied layers, respectively; c_L is the modification factor for flow pressure in the liquefied layer, which is suggested to be 0.3, while that in the non-liquefied layer, c_{NL}, is based on the liquefaction potential index (often denoted as P_L) defined in Iwasaki *et al.* (1978); c_s is the modification factor based on the distance from the waterfront. Suggested values of c_{NL} and c_s are listed in Table 2.

Ashford *et al.* (2011) indicated that the flow pressure approach may be too conservative, *e.g.,* Brandenberg *et al.* (2007), yet can give similar results to flow displacement approach for large ground displacement and relatively strong piles. Notably, the flow pressure approach cannot be applied to the case that all the pile part beneath the crust layer is surrounded by liquefiable soil because no resistance against flow pressure is provided.

Table 2 Modification factors for flow pressure (JRA 2012)

P_L	c_{NL}	Distance to waterfront, s (m)	c_s
$P_L \le 5$	0	$s \le 50$	1.0
$5 < P_L \le 20$	$(0.2P_L - 1)/3$	$50 < s \le 100$	0.5
$P_L > 20$	1	$s > 100$	0

3.1.3 Analysis Models

The analysis presented in this paper focused on Pile #2 because it was the only one modeled in the centrifuge test of Dobry *et al.* (1996) and was more severely damaged in the reality, and also because the flow pressure approach cannot be applied to Pile #1 for its floating in a liquefied layer. Two analysis cases were included: one was to simulate the centrifuge test of Dobry *et al.* (1996) (Fig. 2, yet the analysis model was in prototype scale) for the verification of the modeling, and the other was to simulate the reality (Fig. 1) for discussions on the damage mode of the pile and the action of lateral spreading. The finite element structural analysis software SAP2000 Ver. 20 (CSI 2017) was used. The pile and soil were modeled by the frame elements (for simulating beams and columns) and the 2-joint link elements with multilinear load-displacement relationships (for simulating nonlinear springs) provided by SAP2000, respectively. The settings of analysis models in both cases were separately specified in accordance with the test configurations and the field conditions, and details are given as follows.

The pile in the simulation of the centrifuge test had a length of 10 m (depth range = 0-10 m, in prototype scale) and was elastic with the pile head not axially loaded and free to rotate. Regarding the simulation of the reality, the pile in was 8 m long (depth range = 1-9 m) with a footing connected to the pile head. By contrast to the previous case, the nonlinearity of the pile relevant to its flexural damage was considered using distributed plastic hinges; moreover, the footing (depth range = 0-1 m) was modeled as a rigid beam (for its much larger rigidity than the pile) with a downward load of 290 kN on its top to account for the self-weight of the superstructure (O'Rourke *et al.* 1994), and the rotation of the footing as well as the pile head was not allowed (*i.e.,* so-called fixed-head condition) to approximate the restraint from the column and foundation beams (Fig. 1). The parameters to define the plastic hinges under an axial load of 290 kN are listed in Table 3, where M_{cr}, M_y, and M_u values are according to Meyersohn (1994) and Chang *et al.* (2007), ϕ_{cr} and ϕ_y are associated with an initial and post-cracking $E_p I_p$ values of 18,000 kN-m^2 and 4500 kN-m^2 (Dobry *et al.* 1996), respectively, and ϕ_u was determined following Ko and Lin (2020) considering a displacement ductility ratio of 3 for RC capped piles (Wang *et al.* 2016). Notably, the P-delta effect and large displacement effect were included to account for the possible geometric nonlinearity.

The parameters of the elastic-plastic *p-y* curves in the reality simulation followed Table 1 directly, whereas those for the centrifuge test simulation uses the averages of depth ranges of 0-2 m, 2-8 m, and 8-10 m in Table 1 for the crust, liquefied, and firm base layers, respectively. As for the imposed ground displacement profile for the flow displacement approach, only the linear profile in the liquefied layer (Fig. 4(b) / Eq. (4)) was adopted in the centrifuge test simulation to meet the measured model ground displacement (Fig. 3(a)); the ground surface displacement was 0.8 m, and the displacement decreased to zero at a depth of 8 m (the top of the firm base layer in prototype scale). On the other hand, both cosine and linear profiles (Fig. 4(a) / Eq. (3) and Fig. 4(b) / Eq. (4)) were adopted in the simulation of the reality because the actual distribution is unknown and need investigation; the ground surface displacement was 1.1 m based on the ground surface displacement measured beside NCFH (Hamada 1992), and the displacement decreased to zero at a depth of 8.5 m (the bottom of the estimated liquefied layer). Regarding the flow pressure approach, the pressure profile was determined by Eq. (5) using the same soil properties as those for *p-y* curves. Notably, c_{NL} was specified as 1 considering severe liquefaction with $P_L > 20$, and $c_s = 0.5$ was adopted despite a distance over 100 m from NFCH to the waterfront (Ishihara and Cubrinovski 1998) for conservative reasons.

Table 3 Parameters to define plastic hinge

M_{cr} (kN-m)	ϕ_{cr} (m^{-1})	M_y (kN-m)	ϕ_y (m^{-1})	M_u (kN-m)	ϕ_u (m^{-1})
18.2	0.00101	75	0.0136	86.2	0.182

3.2 1 g Scaled Physical Model Test

To realistically observe the pile-soil interaction during lateral spreading, a 1 g scaled physical model test of a pile loaded by a liquefied and laterally spreading ground was performed, as depicted in Fig. 6. The model pile was based on the NFCH case using a scale factor of 1/17.5. Hence, a high density polyethylene (HDPE) pipe with an outer diameter of 2 cm and a thickness of 0.2 cm was used as the model pile. A four-point bending test indicated that the effective section rigidity of this model pile ($E_p I_p$) is 4.148 N-m^2 at a curvature below 0.8 m^{-1} (the upper bound during this test). The model pile was installed in free-head and end-fixed conditions a model ground with a free face (a riverbank with a retaining wall), as shown in Fig. 6(a).

The model ground was mainly composed of 30 cm-thick uniform fine silica sand, which had a relative density (D_r) of 30% and hence liquefiable as saturated. This liquefiable sand layer was overlaid by a 5 cm thick cemented sand to represent the non-liquefied crust layer, and underlaid by a 5 cm thick filter layer composed of gravel (Figs. 6(a) and 6(b)), making an embedded length of the pile of 40 cm. A liquefaction simulation box developed by Zhang (2023) was used as the container of model ground (Fig. 6(a)). It is a rigid-wall box equipped with a water injection system at its bottom. This system is driven by a constant-pressure pump to cause upward seepage in the soil accommodated in the box. Thus, a quick condition of sandy soil can be achieved to account for liquefaction when the hydraulic gradient is sufficient to reduce the effective overburden pressure to nearly zero, and the lateral spreading of the model ground can be induced.

To check if the model pile and the prototype pile show similar lateral loading behavior, the characteristic value of pile (β) as defined in Eq. (6) was firstly calculated.

$$\beta = \sqrt[4]{\frac{k_h D_p}{4E_p I_p}} \tag{6}$$

The pile can be regarded as infinitely long, or slender, if $\beta L_p > 2.5$ (Poulos and Davis 1980), where L_p denotes the pile length. The k_h value needed for the calculation of β in the physical model was estimated by Eq. (7):

$$k_h = \frac{0.82E_s}{D_p} \tag{7}$$

Based on a strain-controlled cyclic triaxial test on Vietnam sand (D_r = 30%, effective confining pressure = 20 kPa) (Chou 2022), E_s = 2,000 kN/m^2, which was associated with an excess pore water pressure ratio (r_u, denoting the ratio of the excess pore water

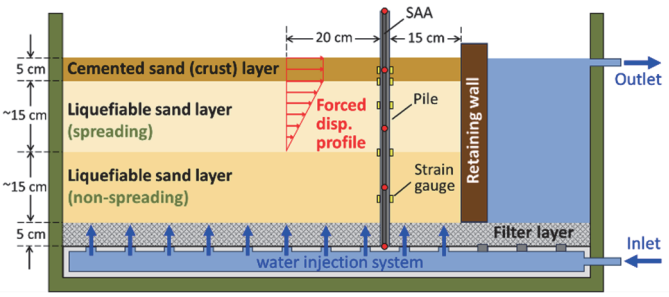

(a) Schematic of test configurations

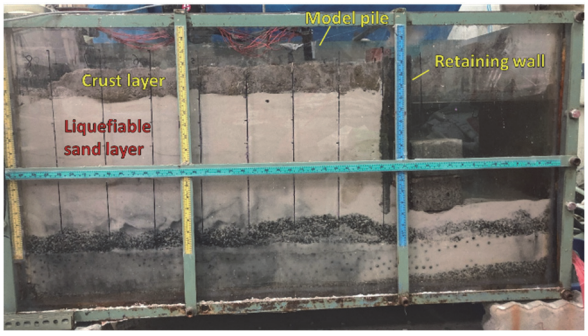

(b) Model condition before the test

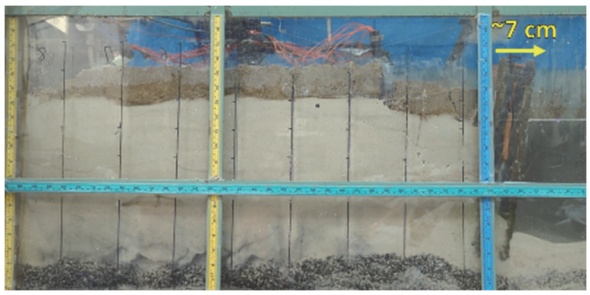

(c) Seepage induced lateral spreading and waterfront displacement

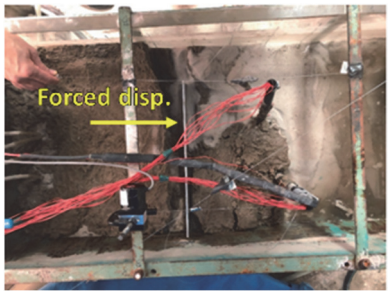

(d) Forced displacement by a penetrated aluminum sheet to approximate a large lateral spreading displacement

Fig. 6 1 g scaled physical model test of a pile loaded by a liquefied and laterally spreading ground in this study

pressure and the effective confining pressure) of 0.95, was adopted for a liquefied model ground in this model test. Then, $\beta L_p = 5.964$ was calculated by Eqs. (6) and (7) for the model pile. Regarding the real pile, if the average of $k_h D_E$ (reduced k_h considering liquefaction) within the pile length was used as representative, $\beta L_p = 3.774$ was obtained. Thus, though the prototype length of 7 m of the model pile was shorter than the real one, both piles can be regarded as slender piles.

During the test, the flexural strains along pile were measured by the strain gauges deployed on both sides of the model pile. Additionally, the shape accelerometer array (SAA), which is basically a series of accelerometers to capture the motion of a slender body, was used to monitor the pile deformation (Fig. 6(a)). Firstly, under the upward seepage, the lateral spreading that occurred spontaneously toward the free face in the depth range from the surface to roughly the middle of liquefiable sand layer, causing a waterfront (the top of the retaining wall) displacement of about 7 cm (Fig. 6(c)). However, the affected range of lateral spreading from the waterfront in this model test was roughly 3 times of the waterfront displacement, much smaller than the range of 10 to over 100 times in several representative historical earthquakes (Ko and Rahayu.J 2022), possibly due to the insufficient level of liquefaction of the model ground. Consequently, despite an interval of only 15 cm from the wall to the pile, the laterally spreading ground induced detectable strains to the pile yet failed to cause a noticeable pile deflection.

To fix this problem, an aluminum sheet was used to penetrate the model ground into the middle of liquefiable sand layer at a distance of 20 cm from the model pile, where can be roughly regarded as a free field. Then, by pulling the top of the sheet, a free-field ground displacement profile which was linear in the liquefiable layer and nearly constant in the relatively rigid crust layer was generated, as demonstrate in Figs. 6(a) and 6(d). During this forced displacement process, the upward seepage was also applied. Thus, the action of liquefaction-induced lateral spreading on the pile is approximated. A ground surface displacement of 5 cm (87.5 cm in prototype scale) was eventually achieved, which deformed the model pile to a level close to the NFCH case.

4. ANALYSIS RESULTS

4.1 Simulation of NFCH Pile #2 Damage: Centrifuge Test (Dobry *et al.* 1996)

Figure 7(a) depicts the displacement and moment distribution along the pile obtained by the flow displacement approach. Notably, because the failure of the pile in the NFCH case was dominated by flexural damage, the shear force distribution is not presented in this paper. The pile exhibited a double-curvature behavior as the moment distribution in the centrifuge test (Fig. 3(b)) implied. The maximum negative moment in the upper part of the pile ($M^{upper}_{\text{max-neg}}$) and the maximum positive one in the lower part ($M^{lower}_{\text{max-pos}}$) both occurred at similar positions as in Fig. 3(b), *i.e.,* near the interfaces of the liquefied layer and both non-liquefied crust and base layers. Moreover, $|M^{upper}_{\text{max-neg}}|$ in Fig. 7(a) is roughly 30% smaller than $|M^{upper}_{\text{max-neg}}|$ in Fig. 3(b), whereas $|M^{lower}_{\text{max-pos}}|$ in Fig. 7(a) is only 7% smaller than $|M^{lower}_{\text{max-pos}}|$ in Fig. 3(b). The former discrepancy may be due to the imperfect modelling of the crust layer. However, both Figs 3(b) and 7(a) show larger $|M^{lower}_{\text{max-pos}}|$ than $|M^{upper}_{\text{max-neg}}|$, and $|M^{lower}_{\text{max-pos}}|$ is corresponding to the largest curvature of the deformed pile in both Figs. 3(b) and 6(a). Furthermore, the pile head displacement in Fig. 7(a) is only 6% smaller in Fig. 3(a).

By contrast, as shown in Fig. 7(b), the flow pressure approach gave a pile deformation curve similar to a cantilever beam and a moment distribution without negative moment in the upper part of the pile though $M^{lower}_{\text{max-pos}}$ was not much different from that in Fig. 7(a). The considerable difference of the analyzed response from the test observation is because the thickness of the liquefied layer was large compared with the pile length, and hence only few soil springs that represented the non-liquefied base layer can provide resistance.

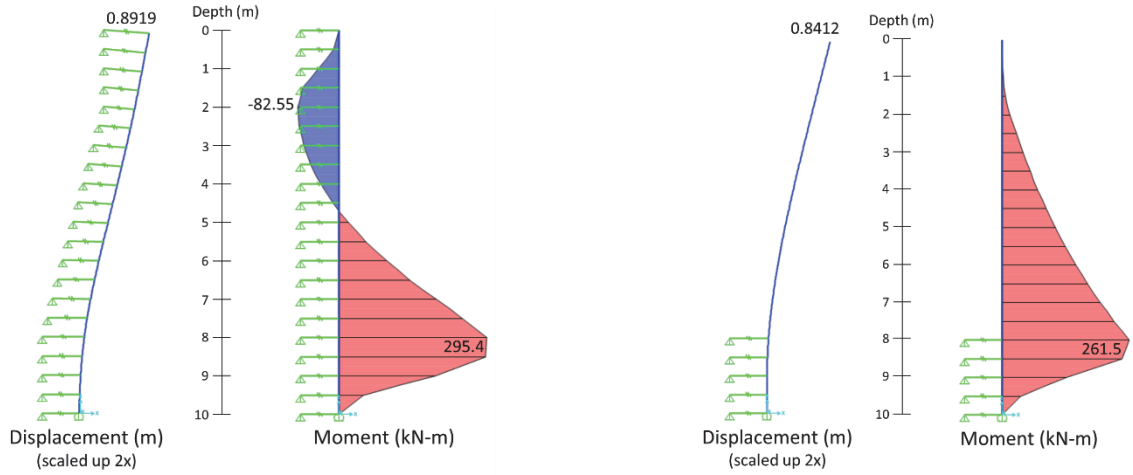

(a) Flow displacement approach (with a linear displacement profile in the liquefied layer) (b) Flow pressure approach

Fig. 7 Pile displacement and moment distribution in the simulation of centrifuge test (in prototype scale)

To sum up, the flow displacement approach with a linear displacement profile in the liquefied layer (just like the test observation) gave satisfactory approximation of the pile response in the test, whereas the flow pressure approach is unpractical when the pile length is so short that only a small portion of the pile penetrates the non-liquefied base layer.

4.2 Simulation of NFCH Pile #2 Damage: Reality

The pile displacement and moment distribution obtained by the flow displacement approach with cosine and linear displacement profiles in the liquefied layer are depicted in Figs. 8(a) and 8(b), respectively. The moment distribution shows that both cosine and linear profiles resulted in a double-curvature behavior of the pile. The non-zero pile head moment was owing to the pile head rotational restraint, which was absent in the centrifuge test simulation. Besides, both caused a pile head displacement close to the applied ground surface displacement (1.1 m). However, the locations of both $M^{upper}_{\text{max-neg}}$ and $M^{lower}_{\text{max-pos}}$ and the magnitudes of $M^{lower}_{\text{max-pos}}$ are rather different. The cosine profile induced $M^{upper}_{\text{max-neg}}$ roughly at the middle of liquefied layer (Fig. 8(a)), leading to yielding of several plastic hinges of the pile at adjacent depths, whereas $M^{upper}_{\text{max-neg}}$ obtained by the linear profile, despite its only slightly larger magnitude, occurred at the interface of the non-liquefied crust and liquefied layers and was sufficient for a plastic hinge of the pile here to reach an ultimate state (Fig. 8(b)). As for $M^{lower}_{\text{max-pos}}$, it was generated at a lower location with a magnitude much smaller than M_y by the cosine profile, whereas the linear profile induced a nearly twice larger magnitude, leading to yielding of the pile at a depth of 7.5 m where slightly above the interface of the liquefied and non-liquefied base layers as the reality.

Notably, after the inclusion of plastic hinges and the pile head restraint, unlike the centrifuges test simulation, the reality simulation gave larger $|M^{upper}_{\text{max-neg}}|$ than $|M^{lower}_{\text{max-pos}}|$, which is agreeable to the actual condition that the upper part of the piles suffered worse flexural damage (Fig. 1(b)). Therefore, the pile nonlinearity and pile head condition are quite influential and hence important in the analysis of laterally load piles. The comparison of the analysis results with Fig. 1(b) further indicates that the linear profile better reproduced the actual position and severity of flexural damage of the pile. Hence, the actual ground displacement profile in the liquefied layer was more likely linear in this NCFH case. However, the appropriate displacement profile may differ from case to case; for example, the cosine profile gave results roughly agreeable with the reality in the analysis of Ko and Lin (2020) on a lateral spreading-induced pile damage case in the 1995 Kobe earthquake. Besides, both profiles gave larger pile head displacement than the actual one, possibly because the lateral resistance of the superstructure and adjacent piles was not modeled in the present study, yet the difference is limited and conservative.

Figure 8(c) shows the results of the flow pressure approach as 17.7% of the flow pressure was applied. At this moment, a pile head displacement of merely 0.135 m were caused, and the induced moment was insufficient to cause yielding. Additionally, the moment distribution, despite the double curvature feature, was largest at the pile head instead of the crust layer-liquefied layer interface. Afterwards, further imposition of flow pressure was inapplicable, and the reason can be explained by the base shear versus pile head displacement curve of this pile, as depicted Fig. 8(d). This curve shows a negative slope after a pile head displacement of 0.135 m, indicating that the pile had a negative stiffness after the status shown in Fig. 8(c). This phenomenon prevented the increase of flow pressure and made the pile become unstable, also reported by Ko and Lin (2020). The negative stiffness can be attributed to the additional moment imposed on the pile head which was generated by the axial load on the footing as the pile head was laterally displaced, that is, the P-delta effect. This effect is often considered equivalent to a reduction of flexural rigidity of a structural member, and hence a negative stiffness, which is regarded as a form of geometric instability, will exhibit as the structural member is sufficiently degraded (Ko and Lin 2020); in this case, the negative stiffness showed after cracking of the three plastic hinges near the pile tip in Fig. 8(c). The geometric instability of this pile occurred before its yielding is because of the rather short penetration depth into the non-liquefied base layer.

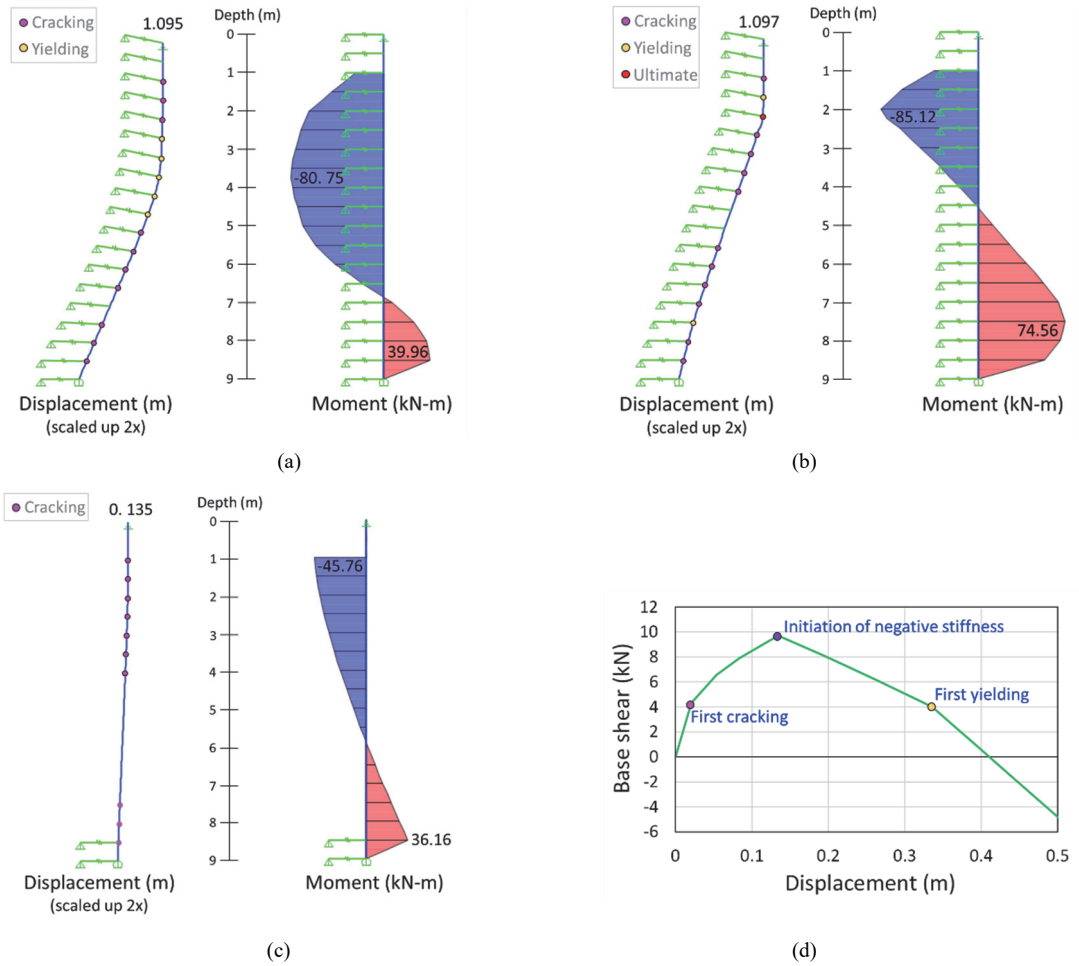

Fig. 8 Pile response in the simulation of the reality: pile displacement and moment distribution (a) by flow displacement (with a cosine displacement profile in the liquefied layer); (b) by flow displacement approach (with a linear displacement profile in the liquefied layer); (c) by flow pressure approach (only 17.7% of the flow pressure was applied); and (d) base shear versus pile head displacement by flow pressure approach

Based on the aforementioned results, the flow displacement approach is again considered more appropriate in simulating the reality NFCH pile damage. Notably, when the linear displacement profile, which gave better approximation in this case, was used, the first plastic hinge of the pile to reach yielding, occurred at the interface of the crust and liquefied layers when the pile head displacement was 0.41 m. On the other hand, yielding initiated at a lower position within the liquefied layer when the pile head displacement was 0.314 m using the cosine displacement profile. This indicate that a fixed-head pile exhibited better resistant performance when the applied lateral spreading displacement profile is linear in the liquefied layer. Moreover, the displacement profile is influential in the location of damage, making it also an important issue in the analysis of piles subjected to lateral spreading.

4.3 Appraisal of Flow Displacement and Flow Pressure Approaches

In the simulation of the NFCH pile failure case, the flow displacement approach gave analysis results that are closer to both the centrifuge test and the reality than the flow pressure approach. The flow pressure approach is a force-based approach. It relies on the availability of an exact equilibrium solution. So, if only a small portion of the pile near its lower end penetrates the non-liquefied base layer or even the whole pile is floating in the liquefied layer, flow pressure approach would be unpractical because the lateral resistance may be insufficient. On the other hand, the flow displacement approach is a displacement-based approach. That is, all the boundary conditions are displacement ones so that a stable equilibrium is always retained unless a total loss of the system stiffness occurs. However, for the possible buckling of a pile due to the loss of lateral confinement from surrounding soil during liquefaction, such as the possible scenario of the Showa Bridge failure in the 1964 Niigata earthquake proposed by Bhattacharya *et al.* (2014), the flow displacement approach is inappropriate because it cannot account for geometric instability. By contrast, the flow pressure approach can be used to deal with geometric instability, such as the negative stiffness shown in Fig. 8(d).

5. TEST RESULTS

5.1 Data Processing

Firstly, the curvature of the model pile at a depth of z can be obtained by the following equation:

$$\varphi(z) = \frac{\varepsilon_L(z) - \varepsilon_R(z)}{D_p} \tag{8}$$

where $\varepsilon_L(z)$ and $\varepsilon_R(z)$ denote the readings of the strain gauges at a depth of z on the left and right sides of the model pile (Fig. 6(a)), respectively.

Then, the moment along the pile can be calculated by $M(z) = EI\varphi(z)$ and can be subsequently approximated by a quartic polynomial:

$$M(z) = a_1 z^4 + a_2 z^3 + a_3 z^2 + a_4 z + a_5 \tag{9}$$

where a_1, a_2, a_3, a_4 are coefficients to be determined by regression analysis, whereas a_5 is set zero because the model pile was in a free-head condition, *i.e.*, $M(0) = 0$.

By differentiating Eq. (9) twice, the soil reaction along the pile can be deduced:

$$p(z) = \frac{d^2}{dz^2} EI\varphi(z) = 12a_1 z^2 + 6a_2 z + 2a_3 \tag{10}$$

Definitions of positive moment and soil reaction for the test setup (Fig. 6(a)) are given in Fig. 9.

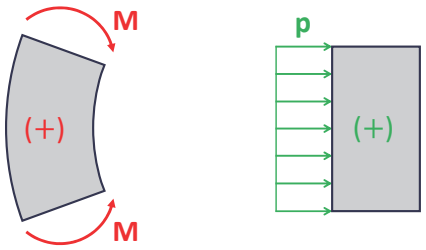

Fig. 9 Definitions of positive moment and soil reaction acting on the pile

5.2 Model Pile Response

Figure 10 shows the displacement distribution obtained by SAA and the moment distribution (both the values calculated based on strain measurement and Eq. (8) and the curve regressed using Eq. (9)) along the model pile. The regression curve is not drawn below the depth of 30 cm. This is because strain gauge data were unavailable there so the function of the regression curve may be invalid in that range. Unlike the centrifuge modelling, the force and stress similitudes usually cannot be achieved in a 1 g scaled physical modelling on geotechnical problems if soil is directly used for the model ground. Hence, the results presented herein are all in model scale, and associated comparisons were made qualitatively.

According to Fig. 10(a), a larger curvature was caused at the lower part of the pile, which is similar to the centrifuge test of Dobry *et al.* (1996) (Fig. 3(a)). The pile head displacement, which was interpolated from the output of SAA, was close to the ground surface displacement (5 cm), implying that it moved together with the crust layer. The moment distribution indicates a double-curvature behavior of the pile with $|M^{lower}_{\text{max-pos}}|$ larger than $|M^{upper}_{\text{max-neg}}|$. This is also similar to the centrifuge test of Dobry *et al.* (1996) and is possibly because the highly flexible HDPE model pile also remained elastic during the test and the pile head was also free. Moreover, the regression moment curve fits well with the values from strain measurement, showing that Eq. (9) is practicable in approximating the moment distribution of a laterally loaded pile.

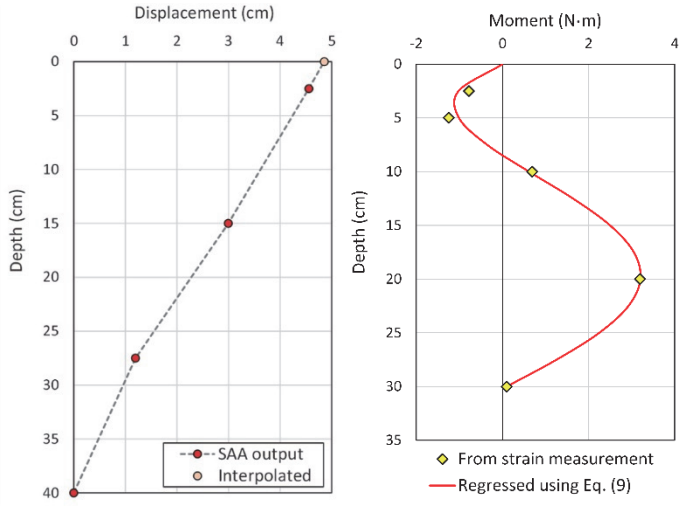

(a) Displacement distribution (b) Moment distribution

Fig. 10 Model pile response in 1 g scaled physical model test at a ground surface displacement of 5 cm

5.3 Comparison of Action of Lateral Spreading on Piles and Moment Distribution along the Pile

Based on the regression moment curve in Fig. 10(b), the soil reaction along the pile can be calculated using Eq. (10), as shown in Fig. 11(a). The definition in Fig. 9 is followed, *i.e.*, positive soil reaction means that soil imposes lateral load to the pile, whereas negative one means that soil provides lateral pile resistance. The pile underwent pressure from the moving soil body from the model ground surface to a depth of about 10 cm, whereas the rest part of the pile above the depth of 30 cm experienced the soil resistance. Part of the reason is the ground was only laterally displaced to a depth of 15 cm. Also, it is possibly because the soil below a certain depth was not completely liquefied and hence might retain certain stiffness and strength.

For further discussions, the axial forces of the soil springs in the reality simulation of NFCH using the flow displacement approach with a linear displacement profile were utilized to calculate an apparent pressure diagram, which is corresponding to the moment distribution in Fig. 8(b). It was then compared with the flow pressure profile suggested by JRA (2012) used in the reality simulation of NFCH to the liquefaction depth (8.5 m), as shown in Fig. 11(b); both can be regarded as the soil reaction along the pile during lateral spreading. In the range of the crust layer (depth = 0-2 m), the apparent pressure from spring forces generally increased with the depth as the flow pressure of JRA (2012) except that near the ground surface, possibly relevant to the rigid footing and pile head restraint. However, the pressure value of the former in the depth range of 1.25-2.25 m was apparently larger mainly because of the inclusion of α_h in Eq. (1b). By contrast, the soil reaction obtained from the test (Fig. 11(a)) exhibited an opposite tendency in the crust layer possibly because the cementation provided some soil strength at a tiny overburden and also because the quadratic

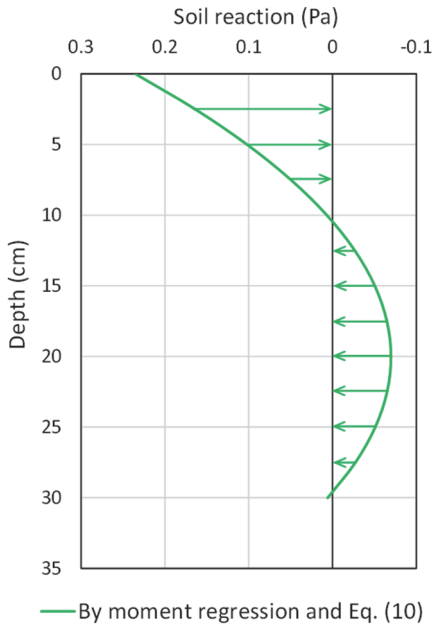

(a) Soil reaction profile calculated by moment regression curve and Eq. (10) in 1 g scaled physical model test

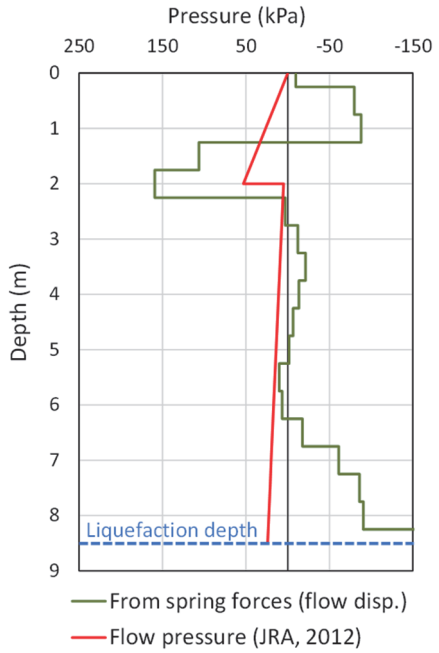

(b) Comparison of the apparent pressure profile from the spring force in the reality simulation of NCFH using flow displacement approach with a linear displacement profile and the flow pressure profile suggested by JRA (2012)

Fig. 11 The action of lateral spreading

Eq. (10) might not approximate the possibly more intense variation. Regarding the liquefied layer, significant difference was noticed between the pressure profiles from spring forces and of JRA (2012); the former represented resistance whereas the latter represented loading. The reason could be the non-zero D_E (0.1) of the *p-y* curves of the soil springs in the liquefied layer (Table 1) and the relative displacement between the pile and surrounding soil that depends on their interaction. Notably, the soil reaction from the test in this range also accounted for resistance possibly due to similar reasons.

To conclude, the action of liquefaction-induced lateral spreading in the crust layer much depends on the factors that may affect the passive earth pressure, whereas in the liquefied layer the level of liquefaction and the pile-soil interaction are quite influential. In this view, the soil displacement approach in which the pile-soil interaction is better considered in the liquefied layer is preferable.

The moment distribution along the pile are also further discussed herein. In the two cases of numerical analysis using the flow displacement approach and the physical model test in the present study, the moment distribution all featured a double curvature. This can be attributed to the restraint from the superstructure and/or the constraint from the crust layer at the pile head and the clamp effect at the pile tip that penetrated the firm base layer. The degree of these effects somewhat altered the distribution tendency. When the pile head was restrained such as in the reality simulation of the NFCH case, the maximum moment in the upper part of the pile tended to be larger than in the lower part compared to the free-head condition such as in the simulation of the centrifuge test (Dobry *et al.* 1996) and in the physical model test in this study. On the other hand, when the pile had a larger penetration length into the non-liquefied base layer such as in the simulation of the centrifuge test (2 m) or even was end-fixed such as in the model test in this study, the maximum moment in the lower part of the pile tended to be larger compared to the case with less end clamp such as in the reality simulation in which the pile only had a penetration length of 0.5 m into the firm base layer. Moreover, all the results in the present studies also indicated that the moment tended to be larger near the interfaces of the crust and liquefied layers and of the liquefied and non-liquefied base layers probably due to the discontinuity in the soil reaction, causing the parts of the pile near these locations more vulnerable to flexural damage.

Similar findings were also reported in other relevant studies, such as several numerical studies on the iconic pile damage case of a three-story building behind a quay wall induced by lateral spreading during the 1995 Kobe earthquake, including the quasi-static analysis using flow displacement approach (Tokimatsu and Asaka 1998; Ko and Lin 2020) and nonlinear dynamic analysis considering the effect of excess pore water pressure (Uzuoka *et al.* 2002). The results of these studies all approximately agreed with the field observations of the damage state (Tokimatsu *et al.* 1997). A shaking table tests on group piles near the waterfront (Motamed *et al.* 2013) with similar configurations to this case also showed roughly conformable tendencies.

6. CONCLUSIONS

In this study, the NFCH pile damage case caused by liquefaction-induced lateral spreading in the 1964 Niigata, Japan earthquake was investigated. The numerical analysis using both flow displacement and flow pressure approaches were performed, and a 1 g scaled physical model test of a model pile embedded in a liquefied and compulsorily displaced model ground was conducted. According to the analysis and test results, the following conclusions can be drawn:

1. The flow displacement approach with a linear displacement

profile in the liquefied layer gave the best approximation of both location and severity of the actual pile damage. The maximum moment and the consequently caused flexural damage is more prone to occur near the interface of liquefied and non-liquefied layers.

2. The flow pressure approach was demonstrated to be inappropriate for the modelling of lateral spreading when the pile does not penetrate deeply into the non-liquefied base layer because in this case only few soil springs can provide resistance.
3. In the flow displacement approach, the displacement profile may influence the damage location and the resistant performance of the pile. Moreover, pile nonlinearity and pile head condition are also important in the analysis of piles subjected to lateral spreading.
4. Using forced displacement of a model ground liquefied by upward seepage to simulate the action of lateral spreading, the behavior of model pile in the 1 g scaled physical model test was similar to that in the centrifuge shaking table test of Dobry *et al.* (1996).
5. The comparison of the soil pressure / soil reaction on piles in the numerical analysis and model test showed that the action of lateral spreading can be considerably influenced by the soil properties and the pile-soil interaction, and hence the analysis should consider these issues as appropriate.

FUNDING

This study was the financially supported by the Ministry of Science and Technology, Taiwan (Research Project MOST 110-2221-E-006-048-MY3).

DATA AVAILABILITY

All analysis and test data generated in this study are included in this paper.

CONFLICT OF INTEREST STATEMENT

The authors declare that there is no conflict of interest.

REFERENCES

AIJ (Architectural Institute of Japan) (2001). *Recommendations for Design of Building Foundations,* Architectural Institute of Japan, Tokyo, Japan (in Japanese).

Ashford, S.A., Boulanger, R.W., and Brandenberg, S.J. (2011). *Recommended Design Practice for Pile Foundations in Laterally Spreading Ground*. Pacific Earthquake Engineering Research Center (PEER), Berkeley, CA.

Bhattacharya, S., Tokimatsu, K., Goda, K., Sarkar, R., Shadlou, M., and Rouholamin, M. (2014). "Collapse of Showa Bridge during 1964 Niigata earthquake: A quantitative reappraisal on the failure mechanisms." *Soil Dynamics and Earthquake Engineering*, **65**, 55-71. https://doi.org/10.1016/j.soildyn.2014.05.004

Brandenberg, S.J., Boulanger, R.W., Kutter, B.L., and Chang, D. (2005). "Behavior of pile foundations in laterally spreading ground during centrifuge tests." *Journal of Geotechnical and Geoenvironmental Engineering*, ASCE, **131**(11), 1378-1391. https://doi.org/10.1061/(ASCE)1090-0241(2005)131:11(1378)

Brandenberg, S.J., Boulanger, R.W., Kutter, B.L., and Chang, D. (2007). "Static pushover analyses of pile groups in liquefied and laterally spreading ground in centrifuge tests." *Journal of Geotechnical and Geoenvironmental Engineering*, ASCE, **133**(9), 1055-1066. https://doi.org/10.1061/(ASCE)1090-0241(2007)133:9(1055)

Chang, D.W., Lin, B.S., and Cheng, S.H. (2007). "Dynamic pile behaviors affected by liquefaction from EQWEAP analysis." *4th International Conference on Earthquake Geotechnical Engineering (4ICEGE)*, Thessaloniki, Greece.

Chiou, J.S., Yang, H.H., and Chen, C.H. (2009). "Use of plastic hinge model in nonlinear pushover analysis of a pile." *Journal of Geotechnical and Geoenvironmental Engineering*, ASCE, **135**(9), 1341-1346. https://doi.org/10.1061/(ASCE)GT.1943-5606.0000015

Chou, B.Z. (2022). *Study on the Relationship between Soil Dynamic Properties, Shear Strain and Excess Pore Water Pressure Using Dynamic Triaxial Test*. Master Thesis, National Cheng Kung University, Tainan, Taiwan (in Chinese).

CSI (Computers & Structures, Inc) (2017). *CSI Analysis Reference Manual for SAP2000 Ver. 20*. Walnut Creek, CA.

Dobry, R., Abdoun, T.H., and O'Rourke, T.D. (1996). "Evaluation of pile response due to liquefaction-induced lateral spreading of the ground." *4th Caltrans Seismic Research Workshop*, Sacramento, CA.

Dobry, R., Abdoun, T.H., O'Rourke, T.D., and Goh, S.H. (2003). "Single piles in lateral spreads: field bending moment evaluation." *Journal of Geotechnical and Geoenvironmental Engineering*, ASCE, **129**(10), 879-889. https://doi.org/10.1061/(ASCE)1090-0241(2003)129:10(879)

Dobry, R., Thevanayagam, S., Medina, C., Bethapudi, R., Elgamal, A., Bennett, V., Abdoun, T., Zeghal, M., El Shamy, U., and Mercado, V.M. (2011), "Mechanics of lateral spreading observed in a full-scale shake test." *Journal of Geotechnical and Geoenvironmental Engineering*, ASCE, **137**(2), 115-129. https://doi.org/10.1061/(ASCE)GT.1943-5606.0000409

Hamada, M. (1992). "Large ground deformations and their effects on lifelines: 1964 Niigata Earthquake." in: Hamada, M., O'Rourke, T.D. (eds), *Case Studies of Liquefaction and Lifeline Performance During Past Earthquakes, Vol. 1, Japanese Case Studies*, Technical Report NCEER-92-0001, National Center for Earthquake Engineering Research (NCEER), Buffalo, NY.

Ishihara, K. and Cubrinovski, M. (1998). "Soil-pile interaction in liquefied deposits undergoing lateral spreading." *XI Danub-European Conference*, Porec, Croatia.

Iwasaki, T., Tatsuoka, F., Tokida, K., and Yasuda, S. (1978). "A practical method for assessing soil liquefaction potential based on case studies at various sites in Japan." *Proceedings of the 2nd International Conference on Microzonation for Safer Construction—Research and Application*, San Francisco, CA, Vol. II, 885-896.

Japan Road Association (JRA) (2012). *Specifications for Highway Bridges, Part V—Seismic Design*. Japan Road Association, Tokyo, Japan (in Japanese).

Ko, Y.Y. and Lin, Y.Y. (2020). "A comparison of simplified modelling approaches for performance assessment of piles subjected to lateral spreading of liquefied ground." *Geofluids*,

2020, 8812564. https://doi.org/10.1155/2020/8812564

Ko, Y.Y. and Rahayu.J, T.K. (2022) "Distribution characteristics of surface displacement due to lateral spreading of liquefied ground." *Journal of GeoEngineering*, **17**(4), 175-187. https://doi.org/10.6310/jog.202212_17(4).1

Lin, S.S., Tseng, Y.J., Liao, J.C., Wang, C.H., and Lee, W.F. (2006). "Ground lateral spread effects on single pile using uncoupled analysis method." *Journal of GeoEngineering*, **1**(2), 51-62. http://doi.org/10.6310/jog.2006.1(2).1

Meyersohn, W.D. (1994). *Pile Response to Liquefaction Induced Lateral Spread*. Ph.D. Dissertation, Department of Civil and Environmental Engineering, Cornell University, Ithaca, N.Y.

Motamed, R., Towhata, I., Honda, T., Tabata, K., and Abe, A. (2013). "Pile group response to liquefaction-induced lateral spreading: E–Defense large shake table test." *Soil Dynamics and Earthquake Engineering*, **51**, 36-46. https://doi.org/10.1016/j.soildyn.2013.04.007

O'Rourke, T.D., Meyersohn, W.D., Shiba, Y., and Chaudhuri, D. (1994). "Evaluation of pile response to liquefaction-induced lateral spread." O'Rourke, T.D, Hamada, M., Eds., *Proceedings of the 5th U.S.-Japan Workshop on Earthquake Resistant Design of Lifeline Facilities and Countermeasures against Soil Liquefaction*, Technical Report NCEER-94-0026, 457-479.

PIANC, World Association for Waterborne Transport Infrastructure (2001). *Seismic Design Guidelines for Port Structures*. A.A. Balkema Publishers, Lisse, Netherlands.

Poulos, H. and Davis, E. (1980). *Pile Foundation Analysis and Design*. John Wiley & Sons, New York, NY.

Railway Technical Research Institute (RTRI) (2012). *Design Standards for Railway Structures and Commentary (Substructures)*. Railway Technical Research Institute, Tokyo, Japan (in Japanese).

Tokimatsu, K. and Asaka, Y. (1998). "Effects of liquefaction-induced ground displacements on pile performance in the 1995 Hyogoken-Nambu earthquake." *Soil and Foundations*, **38**(SP), 163-177. https://doi.org/10.3208/sandf.38.Special_163

Tokimatsu, K., Oh-oka, H., Satake, K., Shamoto, Y., and Asaka, Y. (1997). "Failure and deformation modes of piles due to liquefaction-induced lateral spreading in 1995 Hyogoken-Nambu earthquake." *Journal of Structural and Construction Engineering*, AIJ, **495**, 95-100 (in Japanese). https://doi.org/10.3130/aijs.62.95

Uzuoka, R., Sento, N., Yashima A., and Zhang F. (2002). "Three-dimensional effective stress analysis of a damaged group-pile foundation adjacent to a quay wall." *Journal of JAEE*, **2**(2), 1-14 (in Japanese). https://doi.org/10.5610/jaee.2.2_1

Wang, X., Ye, A., He, Z., and Shang, Y. (2016). "Quasi-static cyclic testing of elevated RC pile-cap foundation for bridge structures." *Journal of Bridge Engineering*, ASCE, **21**(2), 04015042, https://doi.org/10.1061/(ASCE)BE.1943-5592.00007

Zhang, H.Y. (2023). *A Study on the Physical Modelling of Lateral Spreading of Liquefied Ground and Its Displacement Characteristics*. Master Thesis, National Cheng Kung University, Tainan, Taiwan (in Chinese).